Use of Novel Dopants on Solid Oxide Fuel Cell Anodes to Reduce Carbon Deposition and Improve Sulfur Tolerance

Dixon, Rhiannon; Steinberger-Wilckens, Robert

B1206

Use of Novel Dopants on Solid Oxide Fuel Cell Anodes to Reduce Carbon Deposition and Improve Sulfur Tolerance

Rhiannon Dixon, Robert Steinberger-Wilckens
Centre for Doctoral Training in Fuel Cells & Their Fuels
University of Birmingham, Edgbaston, B15 2TT
Tel.: +7815-626-898
RXD130@student.bham.ac.uk, R.SteinbergerWilckens@bham.ac.uk

Abstract

The use of biogas within a solid oxide fuel cell has a number of advantages but poses difficulties in the form of carbon deposition and sulfur poisoning of the anode. As many gas clean-up technologies add large expense to a fuel cell system, thus reducing marketability, this study aims to improve the tolerance of solid oxide fuel cells to these forms of degradation through anode infiltration. Molybdenum and tungsten are commonly used in industrial applications of hydrodesulfurisation and therefore indicate potential for use in solid oxide fuel cell anodes in order to limit the degradation through operation on sulfur-contaminated biogas. Ammonium molybdate tetrahydrate ($(NH_4)_6Mo_7O_{24} \bullet 4H_2O$), ammonium tetrathiomolybdate ($(NH_4)_2MoS_4$), ammonium tungstate pentahydrate ($(NH_4)_{10}W_{12}O_{42} \bullet 5H_2O$) and ammonium tetrathiotungstate ($(NH_4)_2WS_4$) have been used to prepare solutions with which to infiltrate the anodes of Ni/YSZ | YSZ | LSM solid oxide fuel cells. The effects on the rate of deterioration and the microstructure of the anode were studied both electrochemically and qualitatively through Scanning Electron Microscopy (SEM).

1. Introduction

Solid oxide fuel cells (SOFCs) are an energy conversion device capable of achieving over 60% electrical efficiency and up to 88% overall efficiency when used as part of a cogeneration system producing both electricity and heat [1-5]. The combination of high operating temperatures and the choice of materials allows SOFCs to utilise fuels other than pure hydrogen, such as hydrocarbons, biofuels and gasified coal [6]. However, detrimental effects such as carbon formation and sulfur poisoning reduce the durability of the cell and shorten the lifetime.

1.1 Carbon Deposition

The formation of solid carbon on the anode surface of an SOFC can have a variety of consequences ranging from the partial coverage of the surface of the catalyst [7, 8] to the blocking of pores within the anode microstructure. It has been observed that the entire anode channel of a microtubular SOFC was blocked by the formation of carbon when operated on methane only [9]. The issue of carbon deposition can reduce the efficiency of a cell or cause the cell to fail completely, depending on the severity and form of the deposition.

1.2 Sulfur Poisoning

At 800°C, nickel-based anodes are poisoned by H_2S levels as low as 0.05 ppm, with the sulfur tolerance only improving slightly as temperature increases [10] yet most natural gases contain far more sulfur, in the realm of tens to thousands parts per million [11].

Desulfurisation processes can be employed to remove the majority of the sulfur but these processes are not only complex and expensive but also are not capable of continuous removal, thus implying repeated replacement of cleaning cartridges and risk of sulfur break-through. As a result, SOFCs must be adapted to withstand low levels of sulfur without the efficiency of the cell decreasing.

The presence of sulfur directly affects the activity of the nickel catalyst by blocking active sites of the surface which affects the efficiency of both the reforming and oxidation reactions carried out over the catalyst [11]. At fuel cell operating temperatures, the sulfur is commonly adsorbed onto the surface of the nickel catalyst. This is reflected as a fast decrease in the performance which occurs over several seconds before stabilising. This degradation is reversed if the sulfur is removed from the source, as explored by Marina et al. [12].

At lower temperatures, and at higher sulfur content fuels (greater than several ppm), the degradation is not considered to be reversible. This is due to the formation of bulk nickel-sulfur compounds, such as Ni3S2, within the anode which renders the catalyst useless for reforming reactions, though still being effective for hydrogen oxidation.

2. Experimental Procedure

The doping procedure used in this research was reported by Troskialina et al., during the early development of the process [13]. In this work the methodology has been further developed and expanded to include a wider range of dopants. The process involved the creation of a dopant solution by dissolving a salt in an appropriate solvent. This solution

was then applied to the surface of the anode and allowed to infiltrate. Four drops of the solution were applied to the surface, with air-drying, oven drying, and cooling steps between each drop deposition.

The solvent used is determined by the solubility of the salt and the behaviour of the solvent on the anode surface. The basis of this methodology was developed using tin (II) chloride in ethanol. However, the solubility of the different salts often means ethanol cannot be used and other solvents such as water, acetonitrile and dimethylformamide (DMF) have to be emplyed. Table 1 shows the salts and respective solvents used.

Table 1 Salts and Appropriate Solvents using in Creation of Dopant Solutions

Salt	**Chemical Formula**	**Solvents**
Ammonium molybdate tetrahydrate (AMT)	$(NH_4)6Mo_7O_{24} \cdot 4H_2O$	Water
Ammonium tetrathiomolybdate (ATTM)	$(NH_4)2MoS_4$	Water, Acetonitrile, DMF
Ammonium tungstate pentahydrate (ATP)	$(NH_4)10W_{12}O_{42} \cdot 5H_2O$	Water
Ammonium tetrathiotungstate (ATT)	$(NH_4)2WS_4$	Water, Acetonitrile, DMF

The dopant solutions were applied to the surface of the anode in single 32µL drops from a SciPette. The cell was allowed to dry in air for 10 to 15 minutes or until the surface was no longer visibly saturated with liquid. The cell was then transferred to a 120°C oven where it remained for 10 further minutes to completely dry the cell. Upon removing the cell from the oven it was important to allow the cell to cool to room temperature before applying the next drop in order to achieve infiltration of the solution and minimise immediate evaporation. This process was repeated until four drops had been applied to the surface.

Following the doping procedure, the cells underwent calcination in air in a programmable Carbolite furnace. The temperature profile of the programme was determined by the thermal decomposition of the dopant salt in air. The programmes for each salt are shown below in Figure 1.

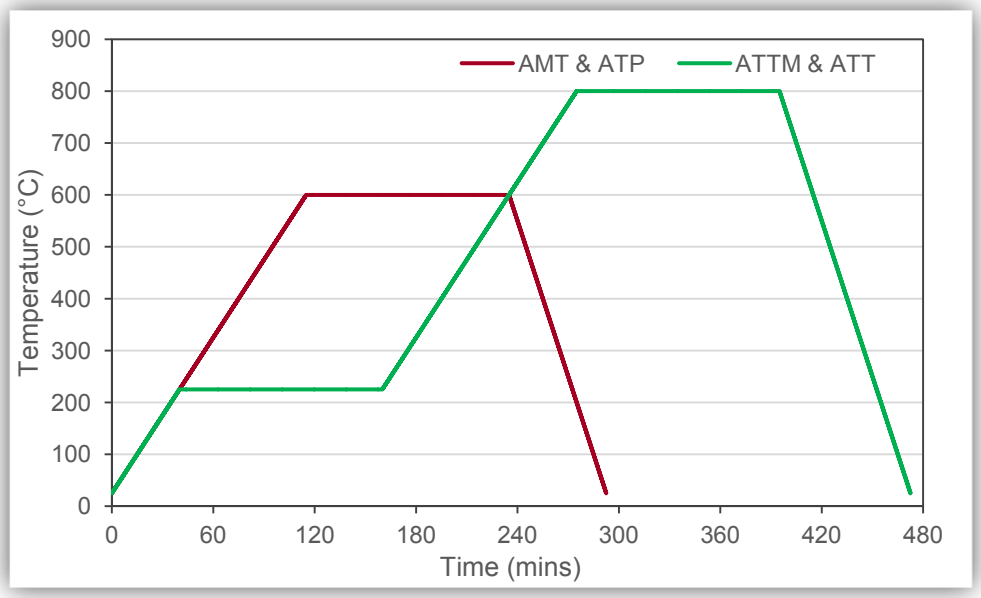

Figure 1: Calcination programmes for AMT & ATP and ATTM & ATT dopes anodes.

3. Results

3.1 Anode Reduction

SEM imaging was used as a tool to qualitatively identify how reduced the cells were after different periods of exposure to a 3:1 ratio of hydrogen to helium. In order to do this a cell was cut into quarters and these set in Buehler EpoThin Epoxy Resin which allowed the cross section to be analysed in a Hitachi TM3030 Tabletop SEM.

The cells purchased from Ningbo Energy Technology Company are not produced with a pore former. In this case the porous microstructure is formed during the reduction of NiO to Ni which has a smaller volume. During fuel cell operation, it is integral than the fuel gas is able to access the triple phase boundary by moving through the porous anode. As a result it is important to fully reduce the anode to make the cell operational.

The cells were placed in a quartz tube within a Vecstar furnace and supplied with a 3:1 ratio of hydrogen to helium once the operating temperature of 750°C was reached. The cells were left overnight, totalling a reduction time of 18 hours.

Figure 2 shows the SEM images of an undoped, AMT, and ATTM doped cells. In all three cases there is a clear distinction within anode microstructures. These images show that each cell is only ~ 50% reduced, leaving a densely packed NiO/YSZ layer between the porous section of the anode and the electrolyte.

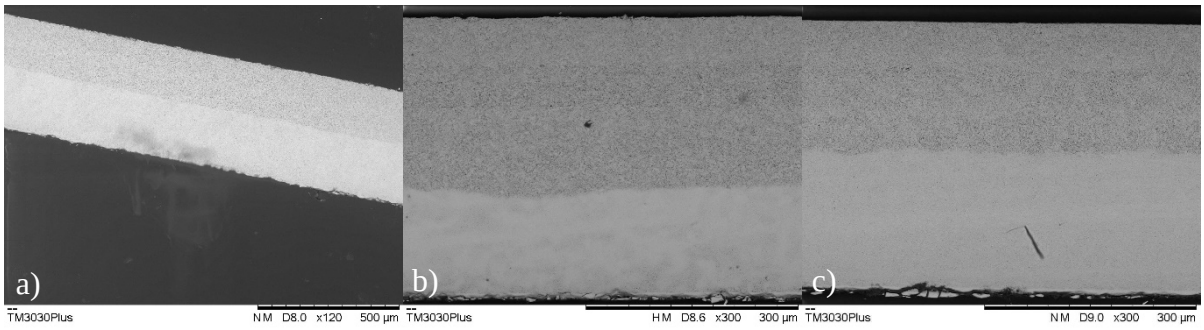

Figure 2 BSE SEM Image of a) Undoped, b) AMT, and c) ATTM doped half cell showing incomplete reduction.

As a consequence of this discovery, experiments were designed to assess how long the cell must be exposed to a 3:1 ratio of hydrogen to helium in order to achieve full reduction. It was postulated that exposing the cells to hydrogen for a longer period would result in better reduction. Furthermore, it was considered that a higher flow rate of gases could result in a higher pressure in the quartz tube which may improve the flow of hydrogen deeper into the microstructure of the anode.

As a result, a cell was reduced at 750°C in a 3:1 ratio of hydrogen to nitrogen, totalling a flow rate of 60 ml/min for 24 hours. This cell was then analysed using SEM, as above. Figure 3 shows the cell at 250x magnification. It is clear that the cell has not completely reduced even under these conditions. However, there are some important differences between Figure 2 and Figure 3. The boundary between the reduced and un-reduced parts of the cell is less defined after 24 hours, compared to 18 hours. The boundary is blurred,

showing an area of semi-reduced NiO, as shown by the decreasing porosity into the cell, as seen in Figure 4. It is less apparent, however, that slightly more of the cell has been reduced under these conditions when compared to the cells reduced for 16 hours.

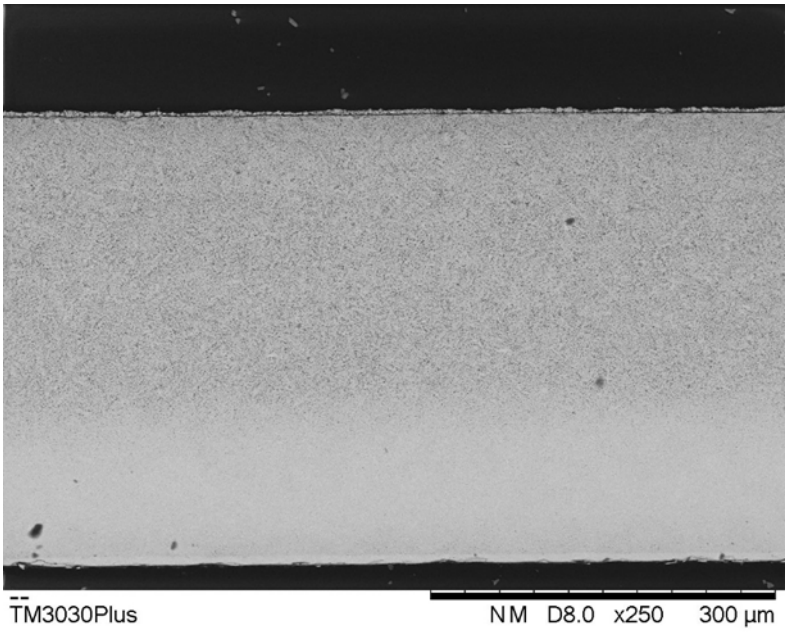

Figure 3: SEM Image of undoped half cell reduced at 60 ml/min for 24 hours.

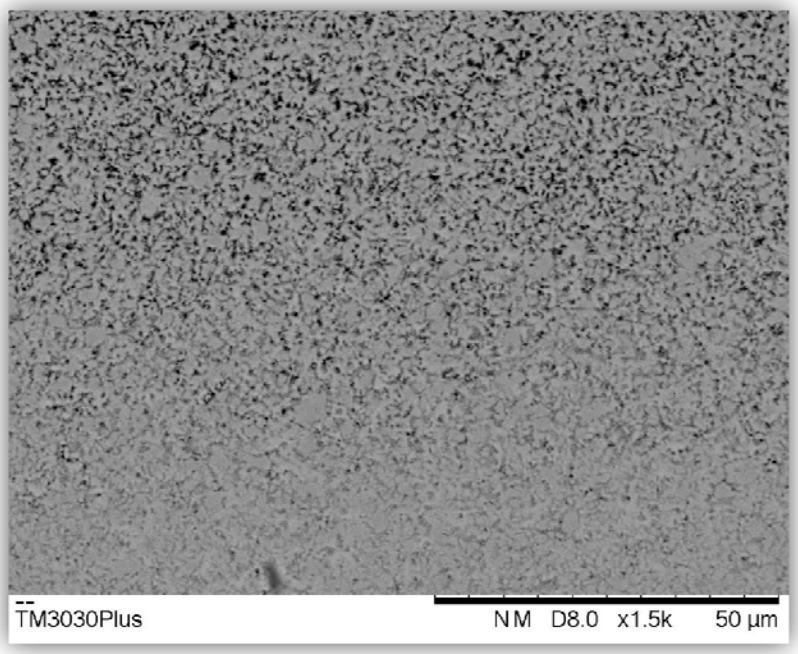

Figure 4: SEM Images of reduction boundary in half cell reduced at 60 ml/min for 24 hours.

The lack of porosity present in the commercial cell serves not only as a barrier to the movement of the fuel gas, but also to the reforming rate of the anode as ~50% of the present nickel is still in the form of NiO. Furthermore, the inadequate formation, or presence, of pores is postulated to detrimentally affect the infiltration of any dopants used.

If only a small number of pores are present in the anode then the dopant solution will saturate the pores more quickly and more solution will be left to dry on the surface of the anode, causing less infiltration to take place.

3.2 Development of Doping Procedure

The doping procedure was developed by Trokialina et al. using a dopant solution of tin (II) chloride in ethanol [13]. As the salts used in this experiment are not soluble in ethanol, other solvents had to be implemented and the procedure needed to be altered accordingly. Ethanol was the optimal solvent to use as it dried rapidly in air and dispersed across the surface of the cell after a drop was applied. Good dispersion of the dopant solution across the face of the cell is integral to achieve an even loading of dopant through the entire anode.

Water was used as the solvent for AMT but due to increased surface tension, when compared to ethanol, the dopant solution did not disperse across the cell once being dropped on the surface. Instead, the solution formed a puddle on the surface. It is clear to see that this behaviour would lead to uneven doping of the anode, with only some parts of the anode being exposed to the dopant.

In order to achieve adequate dispersion across the face of the cell, the surface tension between the surface and the solution had to be reduced in order to permit the solution greater freedom of motion laterally across the surface. This was achieved by applying a small volume of solvent to the face of the anode prior to doping. This was best applied using a small atomizer which provided a mist of solvent across the entire face of the anode. Applying the drop to this sprayed pre-wet surface allowed the dopant solution to move around the surface of the cell, alongside mechanical stimulation, which created more even coverage compared to without the use of the pre-wet, as indicated in Figure 5.

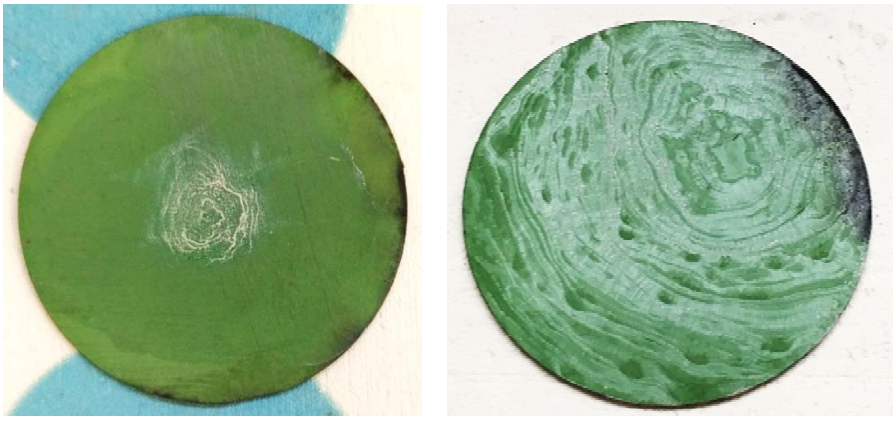

Figure 5: AMT in water a) without pre-wet, b) with sprayed pre-wet.

The pre-wet procedure led to the formation of a ring-like pattern on the surface where the dopant salt had dried as the water evaporated. This was seen, although to a lesser extent, without the pre-wet stage but it is thought that adding more liquid to the surface of the anode causes the pores in the microstructure to become saturated more quickly and therefore not allow for as much infiltration as desired. This is easily overcome through the application of a washing stage where further solvent is sprayed onto the surface of the anode. This dissolves the salt left on the surface and allows more to infiltrate the cell. At this stage it is important to note that the cell is not mechanically disturbed because good

coverage has already been achieved. The washing step visibly reduces the salt left on the surface, as shown in Figure 6, implying that more salt has entered the microstructure of the anode.

Figure 6: Cell from Fig. 6b after washing step.

The pre-wetting spray and washing step have been implemented for all salts and solvents reported here. However, it is worth noting that the results of some cells are different to others. When using the pre-wetting spray method on a batch of cells being doped with AMT in water, the ring-like pattern was not present on every cell, as shown in Figure 7. It is thought that this is due to differing porosities and microstructure between the cells themselves. This is difficult to account for as the cells are purchased rather than manufactured in-house.

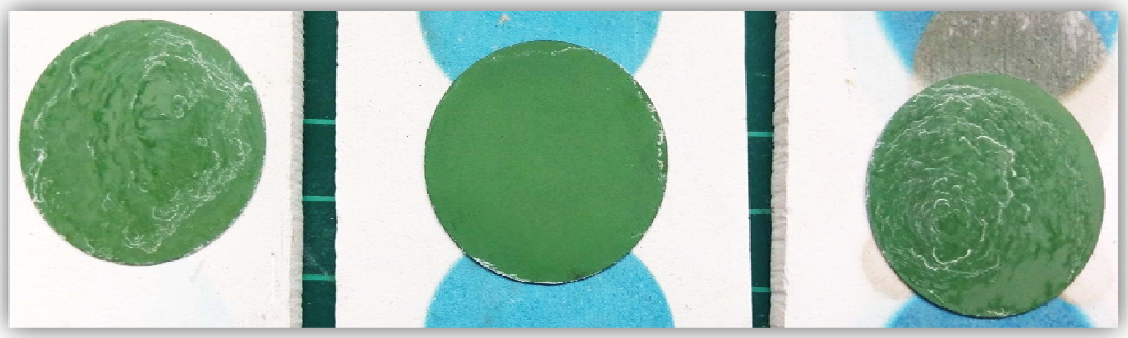

Figure 7: Cells doped with AMT in water with pre-wet spray showing inconsistent ring-like patterns.

3.3 Dopant Penetration

SEM was used to quantify the depth to which the dopant had infiltrated within the anode for each dopant after calcination and reduction had been carried out. This was achieved by using the linescan mode on the Quantax 70 EDX software.

As the doping was carried out pre-reduction, the number of pores was minimal which may also be a barrier to the success of the infiltration of the solution into the anode. Therefore, it was investigated if the penetration of the dopant was improved by doping after reduction.

Figure 8 shows the penetration of molybdenum into the anode when doped with AMT and ATTM. Firstly, it is clear to see that neither dopant has infiltrated the cell as well as desired

as the effectiveness of infiltration decreases with anode depth. In both cells the majority of the dopant was present at the surface of the cell, with a serious drop-off to between 20% and 0%.

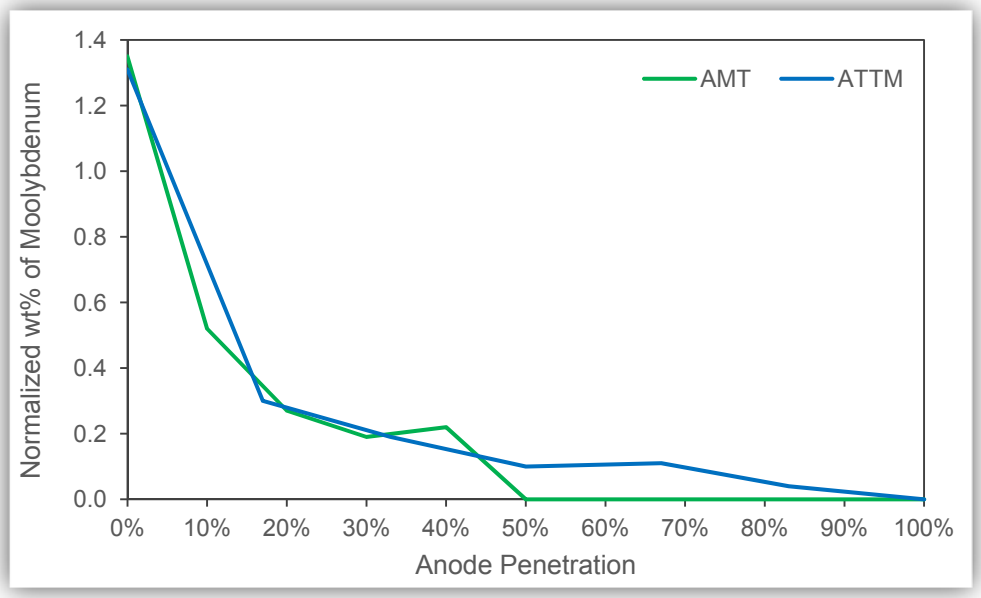

Figure 8: Penetration of AMT and ATTM into half cell.

Whilst both cells showed poor infiltration, the ATTM doped cell showed the presence of molybdenum throughout the entire depth of the anode whereas AMT was only able to permeate up to the reduction boundary, as identified in Section 4.1. This proves that it is important to ensure that the cells become completely reduced as it is possible that during the reduction process the changes in microstructure aid in the infiltration of dopant further into the cell, especially in the case of AMT.

The presence of molybdenum through the whole depth of the anode could be attributed to the formation of MoS2. After calcination and reduction, the AMT should have formed metallic molybdenum and ATTM decomposed to form MoS2. Due to the limitations of SEM/EDX measurements, molybdenum and sulfur cannot be differentiated from each other and so some of the wt% of molybdenum presented may in fact be sulfur. The form of molybdenum in the cell after doping will be analysed and confirmed through XPS and XRD.

The decrease from 1.35 wt% and 1.31 wt% for AMT and ATTM respectively to less than 0.3 wt% indicates that the majority of the dopant metal is present on the surface of the anode, therefore implying that the infiltration has not been particularly effective. This is confirmed by the EDX map of molybdenum presented in Figure 9. This pictorially displays the majority of the molybdenum present is on the surface of the cell rather than dispersed through the anode microstructure. This could be improved by implementing more washing steps to dissolve the salt on the surface and allow it to infiltrate. Conversely, the lack of porosity in the unreduced cell may be proving to be a barrier to the movement of the dopant deeper into the anode.

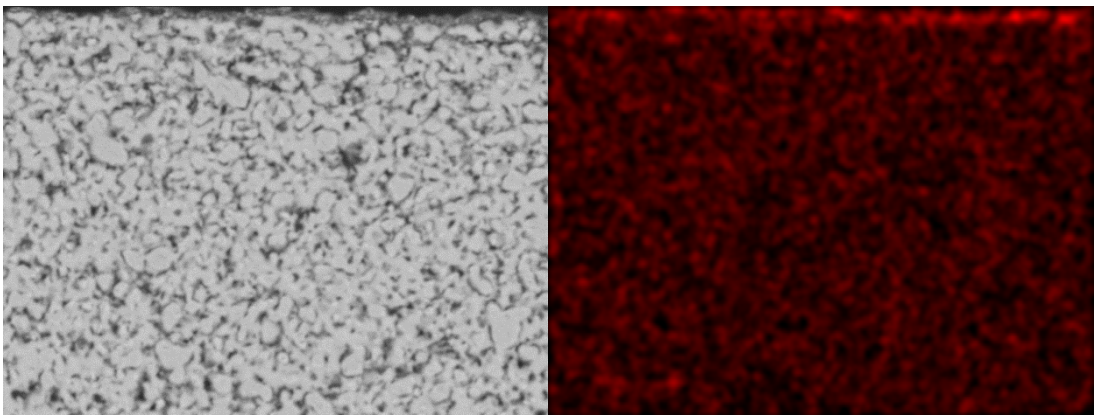

Figure 9: SEM cross section of surface of ATTM-doped half cell and EDX map showing presence of molybdenum.

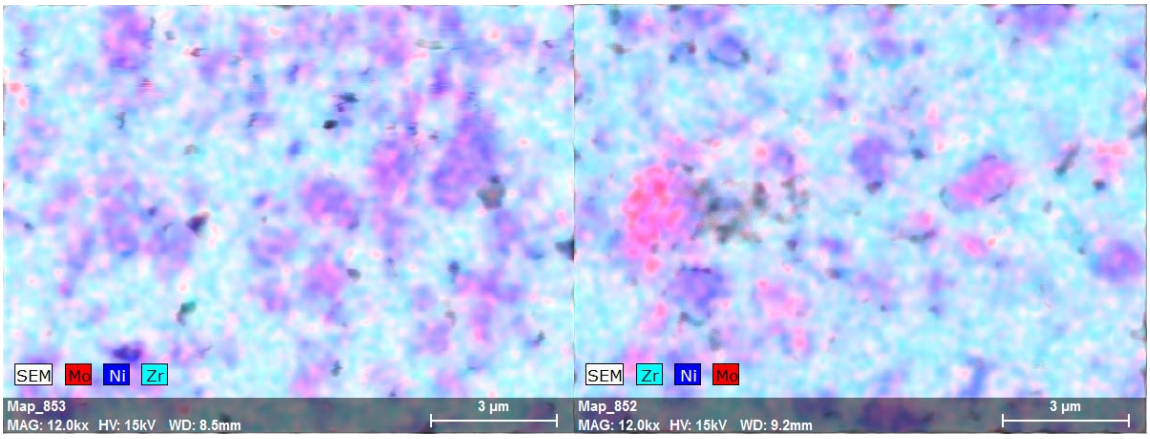

Figure 10: SEM/EDX map of AMT and ATTM doped half cells.

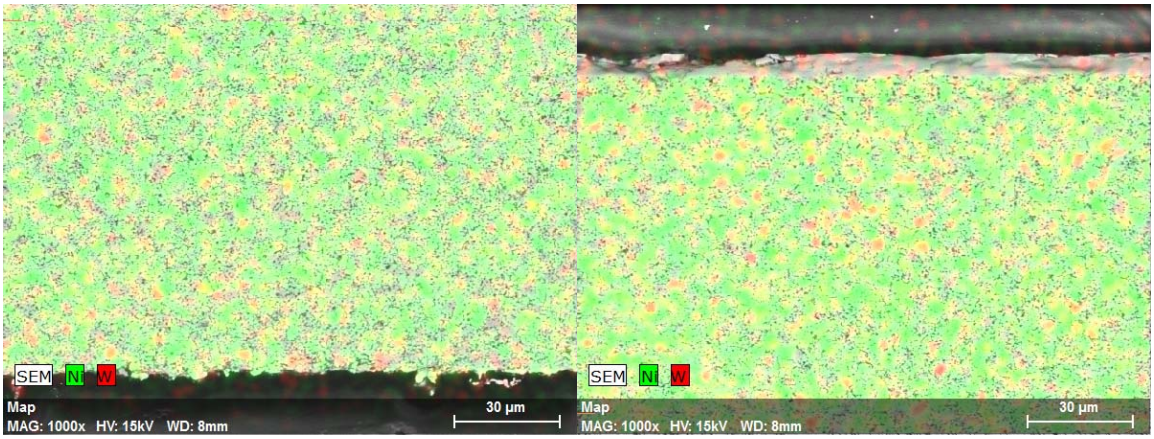

Figure 11: SEM/EDX map of ATP doped half cell (from left to right: top of anode (surface) and bottom).

EDX maps were used to analyse the location of the dopant within the microstructure. Figure 10 shows the position of molybdenum (red) in the nickel/YSZ structure. It can be clearly seen that there are large areas where molybdenum is not present and these represent the YSZ, meaning molybdenum does not seem to be attaching to the YSZ itself. Instead, areas of red are commonly overlapped with areas of dark blue, making the purple

colour present on the EDX maps. This indicates that molybdenum is bonding to the nickel during calcination and reduction and potentially creating a nickel-molybdenum alloy. The location of the dopant within the microstructure is important as the metal must be bound to the nickel catalyst in order to protect it from carbon and sulfur.

EDX was also used to qualitatively assess the presence of tungsten in a cell doped with ATP. As shown in Figure 11, tungsten was much less present in the anode microstructure than molybdenum. Although tungsten was visible, to the eye, on the surface of the anode, the SEM software reported a 0 wt% of tungsten throughout the entire cell. However, tungsten is seen in the EDX maps shown above, indicating small pockets of tungsten have actually infiltrated into the full depth of the anode. It is thought that the concentration of dopant was too low to be detected by the machine available, hence the discrepancy. With tungsten presence as low as this, it is impossible to draw any significant conclusions regarding where the tungsten is bound in the microstructure.

4. Conclusions & Further Work

In this study, the process of doping a Ni/YSZ anode with various molybdenum and tungsten salts has been developed. Appropriate solvents were investigated to achieve a homogenous dopant solution for use in infiltration. Due to issues with solvents and surface tension, a pre-wet spraying step was implemented to ensure proper dispersion of the dopant solution across the face of the anode. Further to this, a washing step was added post-doping to minimise the presence of salt on the face of the cell and promote infiltration into the microstructure.

It was found that the commercial cells used in this study are created without a pore former and that pores in the microstructure were created during the reduction of NiO to Ni. During SEM analysis, it was shown that reducing the cells for 18 hours did not completely reduce all of the NiO, leading to an anode that was not porous throughout. After reducing a cell for 24 hours, under higher gas pressure, the reduction boundary was more blurred but complete reduction was still not achieved.

The success of the infiltration was analysed using SEM and EDX through qualitative assessment of the microstructure and elemental analysis. It was shown that the majority of the dopant was present on the surface of the cells and that infiltration deep into the anode was minimal. This could be due to the incomplete reduction leading to a lack of pores being formed. This could also be due to the absence of pores at the time of doping. Doping after the cell has been reduced will be investigated to assess if the presence of pores during doping causes less saturation of the microstructure by the solvent and better infiltration of the metal throughout the anode.

Furthermore, x-ray photoelectron spectroscopy (XPS) and x-ray diffraction (XRD) analyses will be utilised to investigate the compounds formed after doping. Metallic molybdenum/tungsten and molybdenum/tungsten disulphides should be present in the cell after doping with AMT/ATP and ATTM/ATT respectively. XPS and XRD will also confirm if the dopant has bonded to the nickel catalyst and formed a bi-metallic alloy, as is postulated.

References

[1] A. Faes, A. Hessler-Wyser, A. Zryd, J. Van Herle, “A Review of RedOx Cycling of Solid Oxide Fuel Cells Anode”, Membranes (Basel), **2** (2012) 585-664.

[2] J. Jia, Q. Li, M. Luo, L. Wei, A. Abudula, “Effects of Gas Recycle on Performance of Solid Oxide Fuel Cell Power Systems”, Energy, **36** (2011) 1068-1075.
[3] J.M. Andújar, F. Segura, Fuel Cells: History and Updating. “A Walk Along Two Centuries”, Renewable and Sustainable Energy Reviews, **13** (2009) 2309-2322.
[4] A. Hawkes, M. Leach, “Solid Oxide Fuel Cell Systems for Residential Micro-Combined Heat and Power in the UK: Key Economic Drivers”, Journal of Power Sources, **149** (2005) 72-83.
[5] T. Yen, W. Hong, W. Huang, Y. Tsai, H. Wang, C. Huang, C. Lee, “Experimental Investigation of 1kW Solid Sxide Fuel Cell System with a Natural Gas Reformer and an Exhaust Gas Burner”, Journal of Power Sources, **195** (2010) 1454-1462.
[6] J. Goodenough, Y. Huang, “Alternative Anode Materials for Solid Oxide Fuel Cells”, Journal of Power Sources, **173** (2007) 1-10.
[7] R. Gorte, J. Vohs, S. McIntosh, “Recent Developments on Anodes for Direct Fuel Utilization in SOFC”, Solid State Ionics, **175** (2004) 1-6.
[8] R. Kee, H. Zhu, D. Goodwin, “Solid Oxide Fuel Cells with Hydrocarbon Fuels”, Proceedings of the Combustion Institute, **30** (2005) 2379-2404.
[9] K. Kendall, C. Finnerty, G. Saunders, J. Chung, “Effect of Dilution on Methane Entering an SOFC Anode”, Journal of Power Sources, **106** (2002) 323-327.
[10] Y. Matsuzaki, I. Yasuda, “The Poisoning Effect of Sulfur-Containing Impurity Gas on a SOFC Anode: Dependence on Temperature, Time and Impurity Concentration”, Solid State Ionics, **132** (2000) 261-269.
[11] H. Chen, F. Wang, W. Wang, D. Chen, S.-D. Li, Z. Shao, “H2S Poisoning Effect and Ways to Improve Sulfur Tolerance of Nickel Cermet Anodes Operating on Carbonaceous Fuels”, Applied Energy, **179** (2016) 765-777.
[12] O. Marina, L. Pederson, C. Coyle, E. Thomsen, G. Coffey, “Ni/YSZ Anode Interactions with Impurities in Coal Gas”, ECS Transactions, **25** (2009) 2125-2130.
[13] L. Troskialina, A. Dhir, R. Steinberger-Wilckens, “Improved Performance and Durability of Anode Supported SOFC Operating on Biogas”, ECS Transactions, **68** (2015) 2503-2513.